Journal of Vibration Engineering & Technologies (2025)13:220
https://doi.org/10.1007/s42417-025-01783-z

ORIGINAL PAPER

Effectiveness of Nonlinear Energy Sinks in the Suppression of Stall-Induced Aeroelastic Instabilities

S. S. Bhanav[1] · J. Venkatramani[2] · P. V. Malaji[3] · Grzegorz Litak[4]

Received: 15 August 2024 / Revised: 18 December 2024 / Accepted: 3 February 2025

Abstract

Background Nonlinear Energy Sinks (NESs) have been successfully deployed to control hazardous stall-induced aeroelastic responses.

Purpose This study investigates the effectiveness of NES, its parameters and location on airfoil for optimal suppression of stall flutter oscillations.

Methods A mathematical model encompassing a pitch-plunge airfoil is considered. A NES is attached to the chord of the airfoil. Through succinct numerical simulations, we demonstrate the role of NES in possibly reducing the oscillatory instabilities that arise due to a dynamic stall behaviour.

Results We show that amplitude reductions of 30% are possible upon suitably tuning the NES in both deterministic and stochastic flow cases. Heuristically extending the scope of study to multi-NES resulted in minimal improvement in the suppression of oscillatory instabilities.

Conclusion This is possibly the first study to successfully demonstrate amplitude reductions in stall-induced aeroelastic instabilities using NESs. We believe that the findings presented in this study may augment safer operating conditions for aeroelastic systems fraught with dynamic stall-driven instabilities.

Keywords Stall flutter · Dynamic stall · Nonlinear energy sink

Introduction

With the growing need for slender structures with maneuverability and performance, operating elastic structures under fluid loading is a perfect recipe for encountering dynamical instabilities [1]. The dynamical (aeroelastic) instabilities pose grave risks to the structural integrity by either causing abrupt failure through the first passage of time or due to gradual accumulation of fatigue damage [2]. There has been close attention provided to aeroelastic structures such as aircraft wings, wind turbine blades, helicopter blades, micro aerial vehicles etc., particularly with regards to reporting and investigating potential instabilities [3].

The problem of studying aeroelastic instabilities is a radically different paradigm if nonlinearities and stochasticity are present in the underlying system [4]. While nonlinearities may arise in the structure and/or the flow - identifying these nonlinearities, as well as modeling them,

J. Venkatramani, P. V. Malaji, Grzegorz Litak have contributed equally to this work.

✉ J. Venkatramani
vramani465@gmail.com

[1] University of Adelaide, Adelaide SA 5000, Australia

[2] Department of Mechanical Engineering, Indian Institute of Information Technology, Design and Manufacturing Kancheepuram, Chennai 600127, India

[3] Vibration Energy Harvesting and IoT Laboratory, BLDEA's V.P. Dr. P.G. Halakatti College of Engineering and Technology (Affiliated to Visvesvaraya Technological University, Belagavi), Vijayapur 586101, India

[4] Department of Automation, Lublin University of Technology, Nadbystrzycka 36, 20-618 Lublin, Poland

Published online: 03 March 2025

can be demanding tasks [5]. Usually, structural nonlinearities under attached flow conditions give rise to the classical flutter instability [6] characterized as a phase-locking behavior by Venkatramani and co-workers [7]. Aerodynamic nonlinearities, on the other hand, are more complex and occur due to unsteady separated flow around the airfoil [8] at high angles of attack (AoA). The periodic separation and re-attachment of flow around the airfoil is called dynamic stall, and stall flutter is the instability that arises due to the interaction between the airfoil and the dynamic stall nonlinearity. Typically, onset of dynamic stall is marked by a rise in the lift beyond the static stall angle, mostly due to the formation of a vortex at the leading-edgeof an airfoil. Next, the leading-edgevortex convects towards the trailing edge causing an additional generation of lift, manifesting a delay in stall, while pitching moment reduces sharply. Lastly, the vortex is shed from the trailing edge causing a significant reduction in the lift [7]. To provide a better visualization of this aerodynamic/aeroelastic phenomena to a reader, a schematic of the same is provided in Fig. 1. The aeroelastic outcome of above set of events, i.e. stall flutter is characterised by violent torsional oscillations that occur via a sub-critical Hopf bifurcation [9]. For more details into the numerical representation of dynamic stall and its associated nonlinear dynamics, one can refer to the detailed study carried out by Venkatramani and co-workers [10]. The large amplitudes of oscillation of a structure under stall flutter, as well as the corresponding fatigue damage levels, make stall flutter a more dangerous phenomenon as compared to classical flutter [11].

Stochasticity is yet another complexity that an aeroelastic system is often fraught with. The uncertainty/stochasticity may be present in the structural parameters [12] or the input flow [4, 13, 14]. Given that the in-field conditions are ridden with randomly time-varying wind gusts, it is typical in the hitherto literature to emphasize on

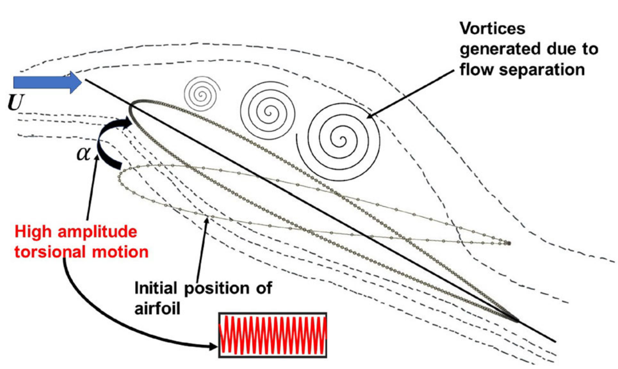

Fig. 1 A schematic of stall instability and flow separation leading to high amplitude torsional oscillations in an airfoil. The streamlines represent the flow of air around the stalled airfoil. Stall instability consists of several stages or modules [8] eventually culminating in dangerous high amplitude stall flutter oscillations

noise-induced instabilities and transitions in nonlinear aeroelastic systems [14]. The impact of these aeroelastic instabilities on the structural integrity cannot be underestimated. Indeed, scenarios involving subcritical transitions [11], transient growth [15], and discontinuity-induced bifurcations [10] exist - more so in stall flutter problems - as illustrated by Venkatramani and co-workers [11, 14]. Such abrupt and premature dynamical transitions accrue large amounts of fatigue damage.

Noting the same, there have been attempts by Venkatramani et al. to develop a suite of measures that can foretell an impending random LCO [2, 16, 17]. However, these methods work only under specific types of *noise-induced intermittency* and only under structural (polynomial) nonlinearities. Attempts were made to use the critical slowing down (presaging a Hopf bifurcation) to warn of catastrophic aeroelastic transitions early [18, 19]. However, these techniques were developed under deterministic conditions under tailored structural nonlinearities. In other words, a generalized aeroelastic instability prediction technique seems to be in its developmental stage in hitherto works [20]. Given that instability prediction in aeroelastic systems - especially under dynamic stall conditions remains elusive, it is pragmatic to counter these instabilities by developing *suppression* strategies. To that end, several methods of suppression of vibratory instabilities have been documented in hitherto literature. Suppression of oscillatory instabilities - both by an active and passive strategy - is ubiquitously found in other engineering systems [21, 22]. Active methods of suppression involve the use of actuators and sensors in a feedback loop, and recent work has also seen the use of proportional-integral observers/controllers [23, 24]. However, active methods take a toll on the aircraft payload [25]. This is accounted for by using passive methods of suppression such as the linear tuned vibration absorber, and the nonlinear energy sink, which are designed as lightweight additions to the primary system - i.e., the airfoil [26].

Success in mitigating aeroelastic instabilities was achieved by using a linear tuned vibration absorber (LTVA) and in turn, showed reductions in LCO amplitude and an improvement in the flutter speed [27]. However, the LTVA lost effectiveness when it was detuned [27]. In order to tackle this problem, the use of a nonlinear energy sink (NES) was proposed. The NES uses an essentially nonlinear stiffness, which allows it to suppress vibrations over a broad band of frequencies [28]. Most of the energy is transferred from the primary oscillator to the NES in a passive and irreversible manner [29, 30]. This is referred to as Targeted Energy Transfer (TET) [26, 31]. This passive method of suppression has been applied in various mechanical systems in several forms [32, 33], summaries of which can be found in [34, 35].

Lee et al. [36] used the NES to suppress LCOs of a pitch-plunge wing section subjected to steady aerodynamics. They showed TET occurs via a 1:1 resonance capture, stating that is feasible to partially or even completely suppress aeroelastic instabilities using the NES. However, the effectiveness of the NES has come into question in recent years on using more rigorous models of aerodynamic loading, such as quasi-steady aerodynamics [37]. Bichiou et al. [37] concluded that the NES has a limited impact on delaying the onset of flutter or reducing LCO amplitudes. Pidaparthi et al. [38] worked on NES designs based on the stochastic optimization approach, and Perez et al. [39] used the genetic algorithm to optimize a flap-NES configuration and showed a reasonable amount of suppression in the oscillation amplitude. Furthermore, [30, 40, 41] demonstrated effective TET in stochastically excited vibrating systems. Wu et al. [42] performed vibration analyses and developed a method for stochastic optimization of NES under random excitation, with some success regarding the effectiveness of the NES as a suppression method.

In the wake of minimal attention devoted so far in suppressing oscillatory instabilities that arise in nonlinear aerodynamic problems such as stall flutter, and noting the importance of the same under stochastic wind conditions, the present study aims to address this end of concern. To that end, numerical simulations are performed in a NACA 0012 pitch-plunge airfoil subjected to nonlinear aerodynamic loads (dynamic stall). The aerodynamic forces are modeled using the well-established Leishman-Beddoes (LB) stall model. We commence the investigations under deterministic conditions. The bifurcation routes are established. Key NES parameters are identified through parametric sweeps. We present scenarios wherein certain pivotal NES parameters, hand-in-hand, with the structural configuration can give rise to considerable amplitude reductions in the instability regimes. Enarmed with these insights, we unravel the effectiveness of NES in suppressing stall-induced instabilities under stochastic wind conditions. We show that the probabilistic nature of the input wind can affect the performance of NES, in turn underscoring the need for further research towards this end. Furthermore, the application of multiple nonlinear energy sinks in aeroelastic problems has been studied in hitherto literature taking into consideration classical flutter by Zhang et al. [43], observing similar TET characteristics and suppression capabilities as the single NES case of Lee et al. [25]. In order to provide a glimpse into possible future work, we study the effectiveness of multiple NESs in a deterministic stall-flutter problem.

The rest of the paper is organized as follows: Sect. “Targeted Energy Transfer” provides a brief introduction to the preliminary ideas of TET and the underlying mechanism behind NES suppression of oscillatory instabilities. Section “Mathematical Model” presents the mathematical model of the aeroelastic system as well as the Leishman-Beddoes model, and the Karhunen-Loeve Expansion for stochastic flows. Section “Methodology” provides insight into the methodology adopted for the study. Section “Results and Discussions” presents and discusses the results obtained. The salient findings that emerge from this study are summarized in Sect. “Concluding Remarks”. Lastly, preliminary studies into a multiNES-Airfoil system are undertaken, and the salient results are outlined in Sect. “Preliminary Study into Multiple NESs”.

Targeted Energy Transfer

Targeted energy transfer (TET) refers to a unidirectional, irreversible transfer of energy from a source to a sink, and is observed in a wide range of physical phenomena [26]. In the case of dynamical systems, TET employs a strongly nonlinear, passive attachment (the NES) to a primary system, in order to drastically alter the dynamics of the same [26]. Upon externally applying loads to the primary system, the NES allows for rapid transfer of energy to itself - from where it is then dissipated due to the damping in the system. The energy transfer is thus directed in a *one-way, irreversible* method. A schematic detailing of the same is provided in Fig. 2. The energy transfer between the primary system and the NES occurs when the instantaneous frequencies of the two approach each other, achieving what is known as internal resonance. Due to the frequency-energy dependency of the NES, the instantaneous frequency of the NES is increased when energy is localized in it, leading to a mismatch of frequencies with the primary system, making the energy transfer unidirectional [44].

In Fig. 2, an NES is attached to the primary system, a linear oscillator (LO). The stiffness and damping coefficients of the LO are k_1 and c_1 respectively, and those of the

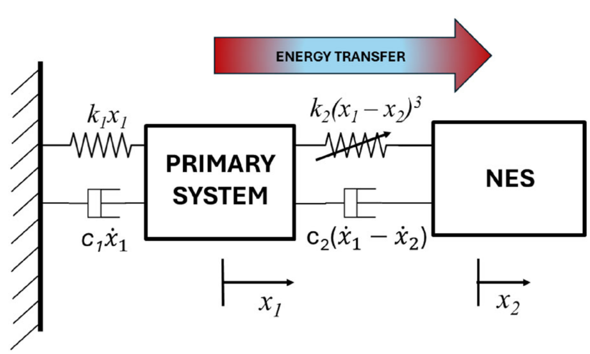

Fig. 2 A sketch of a linear oscillator with NES attached. $x_1, \dot{x}_1, x_2$ and $\dot{x}_2$ are the state variables of the linear oscillator and NES respectively

NES are k_2 and c_2 respectively. We denote the masses of the LO and NES as m_1 and m_2 respectively. The NES is assumed to have no linear stiffness term. The equations of motion of the coupled system are

$$\begin{cases} m_1\ddot{x}_1 + c_1\dot{x}_1 + k_1x_1 + c_2(\dot{x}_1 - \dot{x}_2) + k_2(x_1 - x_2)^3 = 0 \\ m_2\ddot{x}_2 + c_2(\dot{x}_2 - \dot{x}_1) + k_2(x_2 - x_1)^3 = 0 \end{cases} \tag{1}$$

The essential nonlinearity of the NES (provided by the cubic stiffness term) gives the NES leeway in resonance frequency, i.e., there is no single resonance frequency as in the case of tuned mass dampers [45]. This enables the NES to engage in energy transfer across a broad band of excitation frequencies. It helps to note that, analogous to linear normal modes in vibrating systems, there exist nonlinear normal modes (NNMs) - defined as synchronous oscillation of the system [46]. It is the nonlinear interactions between these NNMs and their energy dependencies that play a key role in TET. An in-depth investigation into this is beyond the scope of this study, however, excellent work on the same can be found in [26, 44].

The work of Gendelman, Vakakis and co-workers [47, 48] ascertained that the energy pumping phenomenon in TET was a result of a 1:1 transient resonance capture, i.e., where the internal frequencies of the primary system and the NES match. Subsequently, the NES was applied to Multi Degree-of-Freedom (MDOF) linear oscillators, where it was shown that the NES could separately interact with the multiple linear modes of the system and extract energy from them through a series of *resonance capture cascades*, resulting in robust broadband suppression of oscillations [26].

Deriving impetus from this conclusion, the NES was implemented in several other systems, particularly the Van der Pol oscillator [49], in order to study the NES effectiveness in the case of Limit Cycle Oscillations. On observing suppression of LCOs, the NES was then applied to in-flow airfoils. The NES suppression mechanism was shown to be a series of transient resonance captures between the modes of the wing and the NES, i.e., when the NES and respective modal frequencies match and unidirectional energy transfer is achieved [25].

The application of singular nonlinear energy sinks has seen success in several mechanical systems, prompting the entry of researchers into the avenues of varied NES configurations, including parallel nonlinear energy sinks, or multiple nonlinear energy sinks. Vaurigaud, Savadkoohi and co. have studied targeted energy transfer in such systems both experimentally and theoretically [50, 51], observing robust energy absorption by the parallel NESs.

The equations of motion of the parallel NES coupled system can be obtained as

$$\begin{cases} m_1\ddot{y} + C\dot{y} + Ky + m_{s1}\ddot{y}_1 + m_{s2}\ddot{y}_2 = 0 \\ m_{s1}\ddot{y}_1 + c_{s1}(\dot{y}_1 - \dot{y}) + k_{s1}(y_1 - y)^3 = 0 \\ m_{s2}\ddot{y}_2 + c_{s2}(\dot{y}_2 - \dot{y}) + k_{s2}(y_2 - y)^3 = 0 \end{cases} \tag{2}$$

Parallel NESs work on a similar principle to that of the single NES, where energy transfer takes place from the primary system to the NES via a series of resonance captures. This mechanism is illustrated in Fig. 3. We understand that there exists an activation energy [52] beyond which robust TET occurs and the NES is able to reduce LCO amplitudes. In the case of single NES, there exists only one activation energy level to be achieved for robust TET. On the inclusion of multiple NESs in parallel, we widen the range of initial energy level required to activate the NES [52], thus possibly improving the suppression regime of the NESs. The parallel NESs were primarily introduced to suppress 'high branch responses' [53] which arise from increased excitations of the primary system. Given that the present study deals with stall flutter, which is prone to 'high branch responses' [10, 54] - the premise of using multiple NESs could provide avenues to suppress the high amplitude torsional oscillations that arise with different dynamical signatures.

Mathematical Model

The structure pertaining to the aeroelastic system is considered to be a two dimensional airfoil with pitch and plunge DoFs constrained using torsional and translational springs attached at the elastic axis (see Fig. 4). The NES is modeled as a spring-mass-damper system attached at an offset distance d from the mid chord. The plunge deflection is denoted by h, and α is the pitch angle. The chord length is denoted by c and $b = c/2$ represents the mid-chord length. The elastic axis is located at a distance $a_h b$ from the

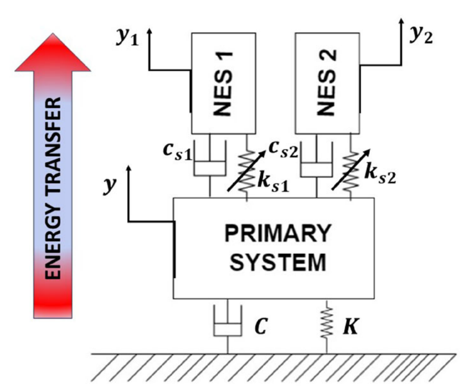

Fig. 3 A representation of a primary system with two NESs attached in parallel. The energy transfer takes place from the region of higher concentration (primary system) to that of lower energy concentration (NESs)

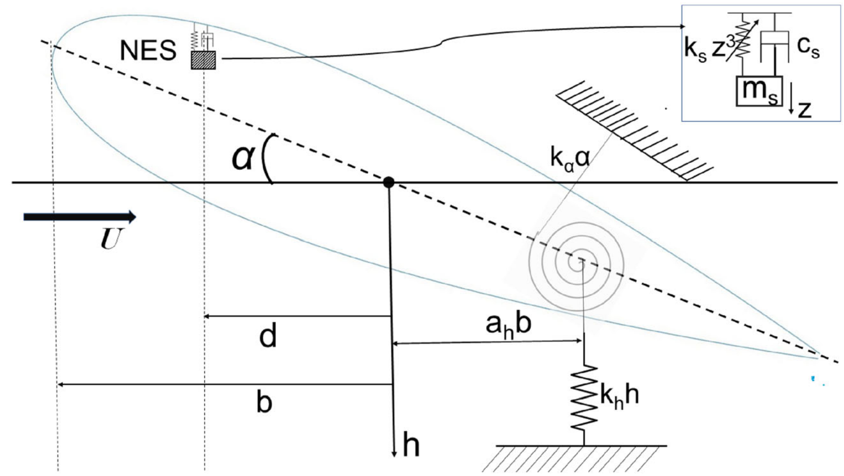

Fig. 4 A sketch of the airfoil section with NES attached. *U* represents the oncoming airflow velocity

mid-chord, while the centre of mass is located at a distance $\chi_\alpha b$ along the chord from the elastic axis.

The NES has an essentially nonlinear stiffness k_s and a linear damping coefficient c_s, and a mass m_s. The governing equations of motion of the airfoil-NES system are given as in [55]

$$\begin{cases} m\ddot{h} + S_\alpha\ddot{\alpha} + k_h h + c_s(\dot{h} + d\dot{\alpha} - \dot{z}) + k_s(h + d\alpha - z)^3 = -L \\ I_\alpha\ddot{\alpha} + S_\alpha\ddot{h} + k_\alpha\alpha + dc_s(d\dot{\alpha} + \dot{z} - \dot{h}) + dk_s(d\alpha + z - h)^3 = M \\ m_s\ddot{z} + c_s(\dot{z} + d\dot{\alpha} - \dot{h}) + k_s(z + d\alpha - h)^3 = 0 \end{cases} \tag{3}$$

Here, the lift L and moment M are functions of the pitch and plunge displacements (α and h respectively), their time derivatives (symbolized by $\ddot{\alpha}$, $\ddot{h}$ and $\dot{\alpha}$, $\dot{h}$) as well as the airflow speed U. Note that L and M effectively represent the aerodynamic forcing, and in this case a nonlinear aerodynamical behavior - dynamic stall - and the mathematical modeling of the same are detailed in the next subsection. These equations are then nondimensionalized. The symbol $''$ indicates a double derivative with respect to time τ given as $\tau = Ut/b$, where U is the dimensional airflow speed, t is dimensional time and b is half-chord length.

$$\begin{cases} \xi'' + \chi_\alpha\alpha'' + \dfrac{\bar{\omega}^2}{V^2}\xi + 2\dfrac{\bar{\omega}}{V}\lambda_s(\xi' + \delta\alpha' - v') \\ \quad + \dfrac{\bar{\omega}^2 b^2}{V^2}\eta_s(\xi + \delta\alpha - v)^3 = -\dfrac{1}{\pi\mu}C_L(\tau) \\ \dfrac{\chi_\alpha}{r_\alpha^2}\xi'' + \alpha'' + \dfrac{1}{V^2}\alpha + 2\dfrac{\delta b^2}{V}\lambda_s(\delta\alpha' + v' - \xi') \\ \quad + \dfrac{\delta\bar{k}}{V^2}\eta_s(\delta\alpha + v - \xi)^3 = \dfrac{2}{\pi\mu r_\alpha^2}C_M(\tau) \\ \in v'' + 2\dfrac{\bar{\omega}}{V}\lambda_s(v' + \delta\alpha' - \xi') + \dfrac{\bar{\omega}^2 b^2}{V^2}\eta_s(v + \delta\alpha - \xi)^3 = 0 \end{cases} \tag{4}$$

Here, $V(= U/b\omega_\alpha)$ is the non-dimensional airflow speed, ω_α is the uncoupled pitch natural frequency, and $\bar{\omega}$ is the ratio of uncoupled pitch and plunge natural frequencies. μ represents the non-dimensional mass of the airfoil, given by $\mu = m/\pi\rho b^2$, where ρ is the density of air, and m is the mass of the airfoil. r_α is the radius of gyration about the **elastic axis given by** given by $\sqrt{I_\alpha/mb^2}$, where I_α is the moment of inertia. S_α **represents the wing static moment about the elastic axis** [1], λ_s (=$c_s/2\sqrt{k_h m}$) and η_s (=k_s/k_h) represent the nondimensionalized damping and stiffness coefficients of the NES respectively. ϵ is the mass ratio of the NES with respect to the wing (m_s/m), and $\bar{k}$ is a constant defined as $b^4(k_h/k_\alpha)$. The offset distance d was normalized by the half-chord length b, to obtain δ. This varies within the range $[-1, 1]$, where -1 and 1 correspond to extreme trailing and leading edges of the airfoil respectively [36]. The non-dimensional structural parameters are chosen from Sai Vishal et al. [10], and are presented in Table 1.

The Leishman-Beddoes Model

The lift and moment coefficients C_L and C_M are estimated using the state-space formulation of the LB model, as it is primarily used in engineering applications [56]. The modeling of aerodynamic loads under dynamic stall conditions involves accounting for different stages viz. flow separation, vortex shedding, and flow reattachment phases, including the loads in the attached flow regime [8]. Indeed, the attached flow regime is accounted for by the Wagner formulation for unsteady aerodynamics,

Table 1 non-dimensional structural parameters of the aeroelastic system [10]

μ	r_α	χ_α	a_h	$\bar{\omega}$
100	0.5	0.25	−0.5	0.2

$$\begin{aligned}C_l(\tau) &= \pi(\xi'' - a_h\alpha'' + \alpha')\\ &+ 2\pi[\alpha(0) + \xi'(0) + (0.5 - a_h)\alpha'(0)]\phi(\tau)\\ &+ 2\pi\int_0^\tau \phi(\tau - \tau_0)[\alpha'(\tau_0)\\ &+ \xi''(\tau_0) + (0.5 - a_h)\alpha''(\tau_0)]d\tau_0,\end{aligned} \tag{5}$$

$$\begin{aligned}C_m(\tau) &= \pi(0.5 + a_h)[\alpha(0) + \xi'(0)\\ &+ (0.5 - a_h)\alpha'(0)]\phi(\tau) + \pi(0.5 + a_h)\\ &\times \int_0^\tau \phi(\tau - \tau_0)[\alpha'(\tau_0)\\ &+ \xi''(\tau_0) + (0.5 - a_h)\alpha''(\tau_0)]d\tau_0 +\\ &\frac{\pi}{2}a_h(\xi'' - a_h\alpha'') - (0.5 - a_h)\frac{\pi}{2}\alpha' - \frac{\pi}{16}\alpha''.\end{aligned} \tag{6}$$

Here, $\phi(\tau)$ is the Wagner function given by $\phi(\tau) = 1 - 0.165e^{(-0.0455\tau)} - 0.335e^{(-0.3\tau)}$. These equations then feed into the ODEs that make up the equations of motion of the system, given in Sect. "Methodology".

The LB model estimates the aerodynamic load coefficients by using the perpendicular and chord-wise components of the force. The load coefficients are given by

$$C_i = g_i(x, \hat{\alpha}, q) \qquad i = c, N, m$$

here c, N, m represent the non-dimensional coefficients of the chord-wise force, normal force, and pitching moment respectively [10]. $\hat{\alpha}$ is the effective angle of incidence given by

$$\hat{\alpha} = \frac{\sin\alpha + \xi'\cos\alpha}{r}$$

The Leishman-Beddoes model was initially developed using experimental data at subsonic speeds [57], and then was modeled in the state-space form [58]. Using the latter, $x = [x_1, x_2 \ldots x_{12}]^T$ are the twelve aerodynamic states. These are then directly coupled with the structural governing equations in the state space form

$$x' = f(x, \hat{\alpha}, q, V, M),$$

Here, V is the non-dimensional flow speed, M is the Mach number and q is the non-dimensional effective pitch rate, given by $q = 2\alpha'$.

The first eight states of x represent the unsteady attached flow regime as mentioned in Eqs. 5 and 6. It is obtained by modifying Wagner's function from the unsteady aerodynamic model [1], and taking into account flow compressibility and the Mach number M. The states x_9, x_{10} and x_{12} model the flow separation regime and represent the delayed normal force component, trailing edge separation point location, and the delayed version of the trailing edge separation point location respectively. State x_{11} accounts for the extra lift generated due to the formation of the leading-edgevortex, when the value of x_9 crosses a certain critical normal force value.

The total loads are given as the summation of aerodynamic forces from the unsteady attached flow regime, the flow separation & reattachment regime and the vortex formation regime.

$$C_n = C_n^I + C_n^f + C_n^v, \quad C_m = C_m^I + C_m^f + C_m^v, \quad C_c = C_c^f. \tag{7}$$

The superscripts, I, f, and v indicate impulsive loads from the attached flow, flow separation, and vortex components, respectively. The aerodynamic load coefficients are thus given by

$$C_N^f = C_N^C\left(\frac{1 + \sqrt{x_{10}}}{2}\right)^2 \tag{8}$$

$$C_m^f = [K_0 + K_1(1 - \hat{x} + K_2\sin(\pi\hat{x}^2))]C_N^C\left(\frac{1 + \sqrt{\hat{x}}}{2}\right)^2 \tag{9}$$

$$C_c^f = 0.97C_{N_\alpha}\left(\frac{C_N^C}{C_{N_\alpha}}\right)^2\sqrt{x_{10}} \tag{10}$$

$$\hat{x} = \begin{Bmatrix} x_{10}, \text{ if } x_{10} > x_{12} \\ x_{12}, \text{ if } x_{12} \geq x_{10} \end{Bmatrix} \tag{11}$$

The state x_{11} accounts for the extra lift generated due to the formation of leading-edgevortex, when the value of x_9 crosses an empirically obtained critical normal force (C_{N1}) value. The coefficients K_0, K_1 and K_2 are experimentally determined coefficients related to the position of the aerodynamic center and the shape of the moment break at stall. The normal force and moment coefficients generated due to leading-edgevortex are given as

$$C_N^v = x_{11} \tag{12}$$

$$C_m^v = \begin{Bmatrix} -\frac{1}{4}\left[1 - \cos\left(\frac{\pi\tau_v}{T_{v1}}\right)\right], \text{ if } \tau_v \leq 2T_{v1} \\ 0, \text{ if } \tau_v \geq 2T_{v1} \end{Bmatrix} \tag{13}$$

Where T_{v1} is the experimentally obtained value of time taken for the leading-edgevortex to travel one chord distance. τ_v is the time that starts when $|x_9| = C_{N1}$ and progresses until reset to 0 by the condition $|x_9| < C_{N1}$. Post this, Eq. 7 sums up the total aerodynamic load coefficients. The equations of motion of the airfoil (Eq. 4) sans NES terms then can be converted into first order ODEs as

$$\begin{Bmatrix} x'_{13} \\ x'_{14} \\ x'_{15} \\ x'_{16} \end{Bmatrix} = \hat{f}(\alpha, \alpha', \xi, \xi', C_l, C_m). \tag{14}$$

Here, the state variables x_{13}, x_{14}, x_{15} and x_{16} represent the pitch displacement and velocity, and plunge displacement and velocity of the airfoil, respectively.

The Karhunen-Loeve Expansion for Stochastic Flows

The fluctuations in the flow are generated using the Karhunen-Loeve expansion (KLE) as in [13, 59]. It is evident that in deterministic settings $V(\tau) = V$, however, in the case of stochasticity, the flow speed is subject to variation with time. These variations are characterized by the noise intensity of the flow, σ as well as the time scale of the flow. The stochastic process is simulated as a bi-orthogonal decomposition of its correlation function, i.e., the oncoming flow is represented as a random process involving an expansion of a set of deterministic functions $v_i(\tau)$ and a vector of independent orthogonal random variables $\eta_i(\theta)$ defined in the probability space (Ω, ξ, P) and $\theta \in \omega$ (where ω is the sample space) [60]. The expression for stochastic flow is [14]

$$V(\tau, \theta) = V_m + \sum_{i \geq 1} \sqrt{\lambda_i} v_i(\tau) \eta_i(\theta) \tag{15}$$

For ease of representation, dependence on θ is ignored in the present work. The deterministic functions $v_i(\tau)$ are obtained by using the Liouville-Neumann series as a solution to Fredholm's equation

$$\int_{\Omega} C(\tau, \tau') v_i(\tau') d\tau = \lambda_i v_i(\tau) \tag{16}$$

where C is the correlation function of $V(\tau)$. We then have an eigenvalue problem where (numerically), **Equation (16) is discretized into matrix form and solved**. The eigenvectors obtained are used as approximations for the eigenfunctions $v_i(\tau)$. We take the number of eigenvalues thus obtained to be n. For the sake of simplicity, the process $V(\tau)$ is assumed to be Gaussian in nature, with a target auto-correlation function

$$R_{VV,tgt}(\tau) = \sigma^2 \exp(-c_1 \tau_{lag}^2) \tag{17}$$

Here, σ is the variance of the process, representative of the noise intensity of the flow. τ_{lag} is the time lag for which the correlation is calculated, and c_1 is the correlation coefficient. The correlation length is defined as the time taken for $R_{VV,tgt}(\tau)$ to go to 0. Lower values of c_1 correspond to longer time scales. Changes in time scales result in production of vastly different dynamical responses, and the present work aims to identify the effect of NES during the interplay of time scales and dynamic stall aerodynamics. The number of terms to be used in Equation (15) is given by finding the minimum number of λ_i satisfying

$$\sum_{i=1}^{z} \lambda_i \geq 0.99 \sum_{i=1}^{n} \lambda_i \tag{18}$$

The variation of flow about a mean flow speed V_m is shown in Fig. 5, along with corresponding plots of the target autocorrelation function as in [60]. Details of the implementation of KLE to simulate randomly time-varying input winds to an aeroelastic system can be found in [13, 60] and are not elaborated here for the sake of brevity.

We further tabulate the noise intensity, time scales and corresponding correlation lengths used in the present work for simplicity (see Table 2).

Methodology

The methodology adopted for the study was as follows - First, we present the aeroelastic response of the system without the NES attachment and compare it with Sai Vishal et al. [10]. Then, the NES is included to the aeroelastic system. The NES parameters for the preliminary study were chosen from existing relevant literature [36, 55] and results are obtained. Keeping the mass, stiffness and damping fixed, a sweep of offset distance (δ) is first performed to tune δ for the given parameters.

It is necessary to clarify at this juncture that the current work aims to study the effectiveness of the NES in the case of stall flutter, and the parametric sweep exercise performed to obtain NES parameters will only provide us with 'tuned' NES parameters. With more in-depth optimization procedures such as evolution or other meta-heuristic methods, it is possible to obtain optimized parameters for the NESs that may further improve LCO amplitude suppression.

Then, for a multi-parameter sweep, the (non-dimensional) NES parameters were considered - mass ratio (ϵ), damping coefficient (λ_s), stiffness coefficient (η_s), and

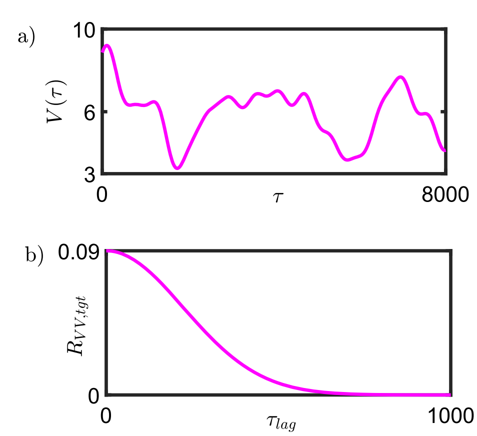

Fig. 5 **a** Flow fluctuations about $V_m = 6$ along with **b** plots corresponding to a correlation length of 1000

Table 2 Parameter values for modeling of stochastic flows using the Karhunen Loeve Expansion [60]

Case	σ	c_1	Correlation Length
a)	0.3	0.001	100
b)	0.3	0.00001	1000

normalized offset distance (δ). As the NES is designed to be a lightweight attachment [26] with a limit on the mass ratio [28], we have limited the NES mass ratio to 10% of airfoil mass. NES stiffness coefficient η_s is varied over a wide range. In order to tune the NES suitably for robust TET, we consider η_s values within the range [10,300]. NES offset distance δ is varied in the range $[-0.9, 0.9]$ following the nondimensionalizing in Sect. "Mathematical Model". Varying the NES offset δ has shown to have an impact on the extent of suppression of LCO amplitudes [37, 55]. The present work uses these parametric sweeps to find an ideal location for the NES through a tuning process.

Through the sweeps, by varying stiffness and damping of NES we aim to find an ideal NES offset δ due to a twofold reason - firstly, in aeroelastic systems, parameters such as placement of elastic axis and distances from mid chord weigh in heavily on the response dynamics of the system [1, 8], and thus the placement of NES at different distances from the mid chord can bring about unprecedented system dynamics along with possible amplitude reduction. Secondly, from a practical standpoint, it is more pragmatic to find an offset distance for a given set of NES stiffness and damping parameters as it is easier to modify and adjust the same.

In the deterministic case, bifurcation diagrams are presented along with time-histories of the system responses with and without the NES. As stall flutter is a pitch-dominant instability, i.e., characterized by violent torsional oscillations [1], the bifurcation diagrams presented are of pitch amplitude (α) with flow speed V as the control parameter. The sweeps are performed with the aim of reducing the same.

Note that we refrain from presenting the responses of the system at higher flow speeds. This is in order to account for the concerns regarding the accuracy of the LB model at α values greater than 40°, beyond which there is a lack of availability of empirically obtained parameters [7, 60]. Using the tuned NES parameters from the sweeps performed in the deterministic case, the airfoil-NES system is then subjected to stochastic flows. In this paper, we consider the findings of Tripathi et al. [60], where the structurally linear airfoil was subjected to nonlinear aerodynamic behavior (dynamic stall) using the LB model, and the stochasticity in the flow was modeled using the KLE. It is noted that the presence of stochasticity largely alters the behaviour of the system, even advancing the onset of instabilities and are in-line with the existing notions in the literature [4, 13, 14]. We attempt to use the NES to study its impact on the system responses.

In real-life conditions, flows comprise various time scales as well as intensities. As in Venkatramani et al. [13], the time scale of fluctuation can be classified into 'short' and 'long' time scales depending on the correlation length. In the present work, a noise intensity of $\sigma = 0.3$ is considered, along with flows varying with long time scales, as in Fig. 5. These are classified as 'long' depending on the system time scale τ_{sys}, which is found to be 70 [60]. Thus, our selected time scale corresponds to a 'long' time scale due to its correlation length of 1000. The performance of the tuned NES is studied with regard to this. Note that this study refrains from invoking vertical turbulence - as an additive noise term [4], as well as presenting a detailed probabilistic characteristic evolution of the input stochastic wind. We believe that this would yield into a significant transgression into characterizing noise-induced transitions in the aeroelastic system than the chosen focus of suppressing oscillatory instabilities.

Results and Discussions

This section is divided into three subsections based on the nature of loading the airfoil-NES system is subjected to. Sect. "Airfoil-NES Subjected to Deterministic Flows" deals with deterministic flows and tuning the NES to provide reduced stall flutter amplitudes. The subsequent subsection deals with implementing the tuned NES in a stochastic loading case in order to understand the effectiveness of NES in cases more similar to real-life scenarios. Finally, preliminary investigations into the effectiveness of multiple NES are presented.

Airfoil-NES subjected to deterministic flows

We begin by presenting and discussing the response of the system when uncoupled with the NES. The bifurcation diagram and time history are presented in Fig. 6. The system parameters (Table 1) are chosen from the work of Sai Vishal et al. [10], and the response obtained is in agreement with the same.

The system initially shows a fixed point response for flow speeds up till the branch point of $V = 5.6$. The system then transitions via low-amplitude LCOs into a regime of aperiodic responses as can be seen in. The second transition is observed at $V = 6.7$, where the system displays high amplitude stall flutter LCOs. Sample time histories

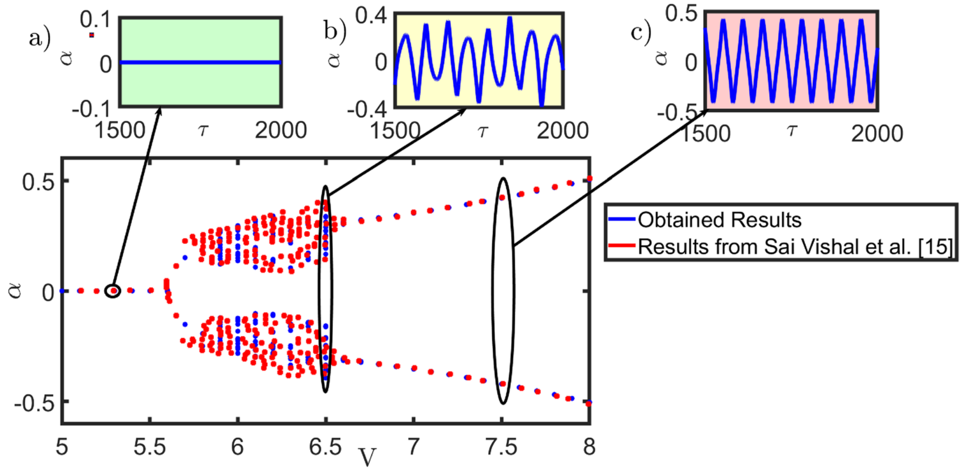

Fig. 6 Base-line bifurcation plot of airfoil subjected to dynamic stall without NES, in comparison with the results of Sai Vishal et al. [10]. Initial conditions are $\alpha(0) = 15°$, $\alpha'(0) = 0$, $\xi(0) = 0$, $\xi'(0) = 0$. Time histories corresponding to **a** fixed point response **b** aperiodic behaviour **c** stall Flutter LCOs

corresponding to fixed point response, aperiodic regime as well as full-blown stall flutter are provided in Fig. 6a, b and c respectively. The peak amplitude continues to increase as flow speed is increased. These sudden transitions arise due to the discontinuous nature of the dynamic stall event. Discontinuity-induced bifurcations [10] are extremely harmful to structure safety due to the abrupt jumps in system response. The high amplitude torsional oscillations and the consequent torsional stresses were also shown to be particularly influential in dictating the extent of fatigue damage accumulation in the system [60]. Deriving impetus from the same, we attempt to use the NES to suppress the pitch LCOs.

In order to obtain preliminary results, we chose parameters by drawing on the conclusions reached in relevant literature [36, 55], provided in Table 3.

On plotting the peak amplitudes versus flow speed, we obtained the bifurcation diagram as in Fig. 7. The reduction in amplitude was found to be minimal, only a 5% reduction was observed. In this retrospect, the reader must cautiously underscore the role of varying the NES parameters toward obtaining considerable reductions in oscillatory instabilities [55]. Keeping this in mind, we in the upcoming parts, proceed to tune the NES parameters and later show that tuned NES parameters can suppress stall-induced flutter instabilities even up to 30 %. In Fig. 7, there is a slight postponement of the initial transition to aperiodic regime, now occurring at $V = 5.8$ instead of $V = 5.6$ as in the uncoupled case. Delays of instabilities were observed in cases of classical flutter as well [55], where the flutter speed was observed to have increased on addition of the NES.

Table 3 non-dimensional NES parameters [36, 55]

ϵ	λ_s	η_s	δ
0.15	0.5	50	−0.5

In order to improve the performance of the NES for the above case, the NES mass, damping and stiffness are kept fixed as in Table 3, and a sweep of NES offset δ is performed at a flow speed of $V = 7.5$. This flow speed is chosen as it is well within the stall flutter regime as seen in Fig. 6. We identify the best value by choosing that δ which corresponds to the least value of peak pitch amplitude α. It helps to note that in the case of airfoil uncoupled with NES, the peak pitch amplitude at a flow speed of $V = 7.5$ was 0.42 radian [10].

We found that the value of δ corresponding to the least peak pitch amplitude (demarcated in Fig. 8) was $\delta_{opt} = -0.3$. In the case of steady aerodynamics as studied by Lee et al. [25], negative NES offset values seemed to show robust LCO amplitude suppression as compared to positive values. Note that we have in comparison a complex and accurate aerodynamic model (LB model) and interestingly our findings of a negative offset distance seems to corroborate with that found in [25]. Next, using the obtained NES offset value, we compare the bifurcation behaviours of the coupled and uncoupled cases; see Fig. 9.

There is a noticeable improvement in terms of decrease in LCO amplitude from that in Fig. 7. The transition to stall flutter beyond the aperiodic regime is also postponed slightly, to a flow speed of $V = 7.2$ as compared to $V = 6.7$ in the uncoupled case.

Furthermore, we observe from Fig. 8 that there are certain δ values that seem to increase the peak pitch amplitude beyond that of the uncoupled case. A similar observation was made by Lee et al. [36], where certain NES parameter values caused the amplitudes of LCOs to grow larger than in the uncoupled case. It was suggested that this may be due to the NES being unable to prevent a sustained resonance capture between the pitch and plunge modes of the airfoil in the case of classical flutter.

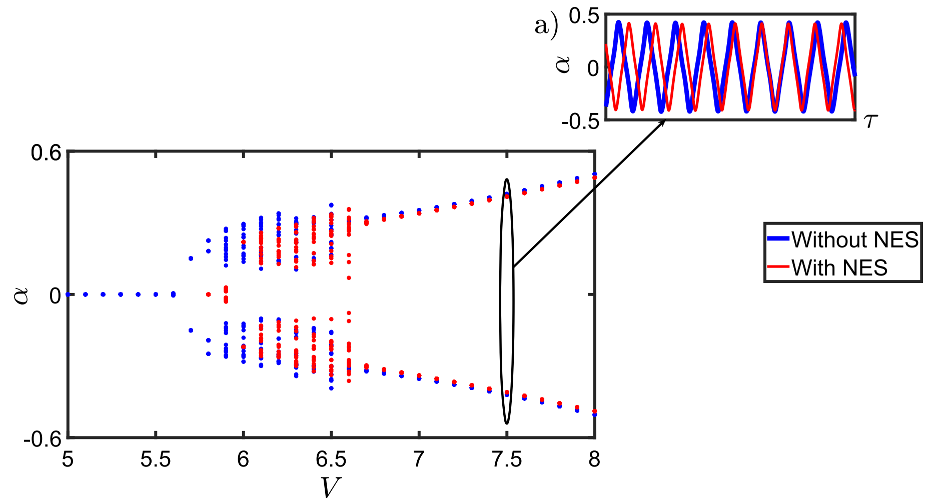

Fig. 7 Comparative bifurcation diagram obtained on using parameters from Table 3. **a** Time history of response at a flow speed $V = 7.5$

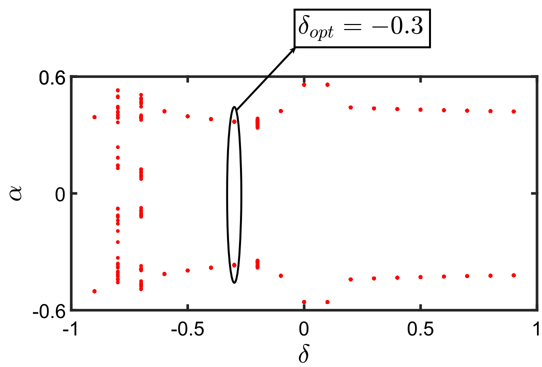

Fig. 8 Peak pitch amplitude α vs NES offset δ

Malatkar and Nayfeh [61] studied the dynamics of the coupled system of Jiang et al. [62], and found that the addition of the NES to the linear structure may lead to an increase of amplitude instead of a decrease, over certain frequency regimes. However, the rebuttal provided by Vakakis et al [63] indicated that optimization of NES parameters was required for maximising energy transfer and reduction of vibration amplitude. In response to this, Malatkar and Nayfeh [64] provided further results indicating that weak coupling of NES to a forced linear oscillator would lead to an increase in amplitude of oscillations rather than a decrease via one way energy transfer in lightly damped subsystems. It is speculated that this is also due to the inability of the damping component to effectively dissipate the localized energy in the NES. Work on the effectiveness of NES in various problems has continued to be studied, and frequency regimes of robust suppression are observed, indicating that parametric optimization of the NES will allow for improved TET.

In the case of stall flutter, the pitch-dominant nature of the instability suppresses the natural dynamics of the plunge mode, and the pitch mode draws energy from the flow and transfers it to the plunge mode [7, 11]. We must suitably tune the NES to attempt to jeopardize the coalescence of pitch and plunge frequencies [65] and prevent

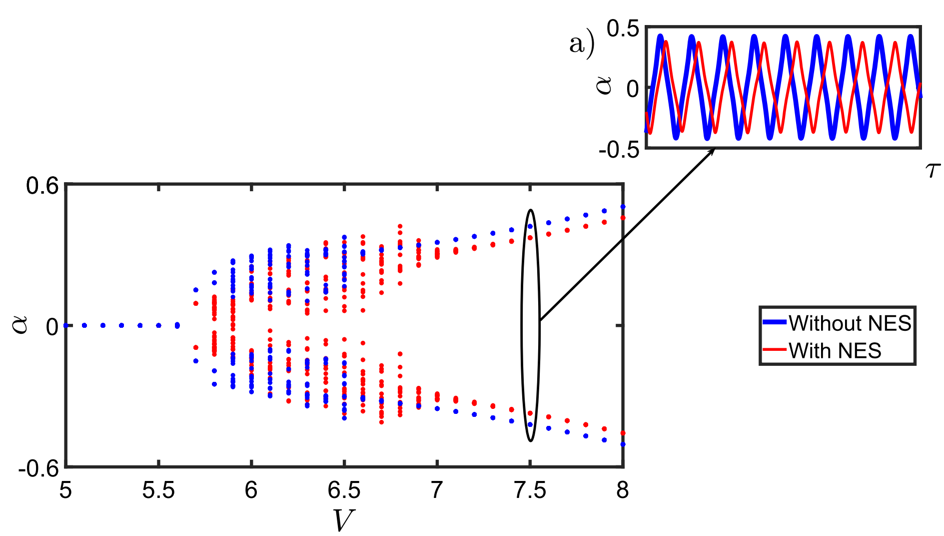

Fig. 9 Comparative bifurcation diagram after using $\delta_{opt} = -0.3$. **a** Time history of response at flow speed $V = 7.5$

direct energy transfer during stall flutter. This process of tuning the NES is achieved by performing a multi-parameter sweep of NES parameters and finding parameters that lead to robust NES performance. The effect of NES mass ratio with regards to NES performance has been studied in the literature [41, 66], indicating that suppression as well as increase in flutter boundary improves with higher mass ratio values. However, keeping practicality in mind, we limit ϵ to 10% of the airfoil mass. In the following sweep presented in Fig. 10, we vary the values of NES damping while attempting to locate a 'tuned' value of NES offset for each of the parameter sets. The parameter values can be found in Table 4.

The above cases were chosen to represent a larger sample of data obtained over several sweeps, which have been omitted for the sake of brevity. We notice in Fig. 10a that for NES locations near the mid chord (which corresponds to $\delta = 0$), the peak responses are aperiodic in nature. Considering that the sweeps were all performed at a flow speed of $V = 7.5$, well within the stall flutter regime (see Fig. 6), it can be inferred that the NES placed at those locations will induce aperiodic behaviours in the system at that flow speed.

Furthermore, on increasing the damping coefficient value to $\lambda_s = 0.03$, there was a comparable decrease in pitch amplitude, which now fell to 0.36 radian. We also note that some of the NES offset locations which previously gave rise to aperiodic behaviour, did not once the damping was increased. This could indicate that the NES is both effectively transferring as well as dissipating energy from the primary system due to the increased damping, without allowing the localized energy to leak back into the primary system. Seeking the possibility to further the extent of LCO amplitude reduction, we sweep through higher values of NES stiffness, the results of which are presented below in Fig. 11.

The significant reduction in LCO amplitude suggests that higher NES stiffness values provide better means for the energy transfer from the primary system to the NES [41]. Furthermore, the need for higher damping values is also displayed as it will reduce the introduction of aperiodic behaviour in the stall flutter regime at particular offset locations. To that end, we set a high NES damping value of $\lambda_s = 0.1$ and perform sweeps of NES stiffness. The results of the sweep are provided in Fig. 12, along with the table of parameter values corresponding to the figure in Table 6.

It was noted that the trends with regards to NES offset were initially in agreement with the literature [36, 67] - negative values of δ showed better suppression. However, with increase in stiffness, the tuned NES location shifted closer to the nose of the airfoil. This may be attributed to the effect of mass distribution within the airfoil due to the inclusion of the NES, as mass balancing is known to have a large impact on flutter speed and amplitude [1].

The least peak pitch amplitude was obtained using parameters from case (c) in Table 6, corresponding to Fig. 12c. These parameters were then chosen and a

Table 4 Parameter Values for the sweep results in Fig. 10. The corresponding minimum peak pitch amplitude is also denoted

Case	ϵ	λ_s	η_s	δ_{opt}	$\min(\alpha(\tau))$ [rad]
a)	0.1	0.01	80	−0.4	0.40
b)	0.1	0.03	80	−0.1	0.36

Table 5 Parameter values for sweep with high values of NES stiffness corresponding to Fig. 11. Minimum peak pitch amplitude is also denoted

Case	ϵ	λ_s	η_s	δ	$\min(\alpha(\tau))$ [rad]
a)	0.1	0.03	130	0	0.35
b)	0.1	0.03	170	0.2	0.33
c)	0.1	0.03	200	0.2	0.33

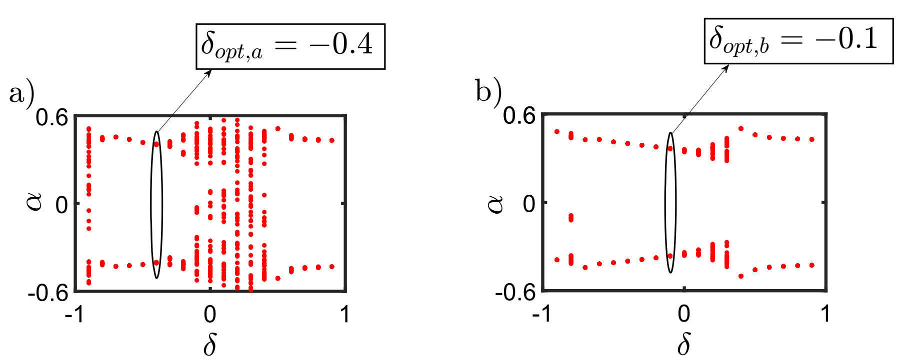

Fig. 10 Sweep Results on varying NES damping. Tuned δ values for Cases **a** and **b** in Table 4 are identified by sweeping for the lowest amplitude value

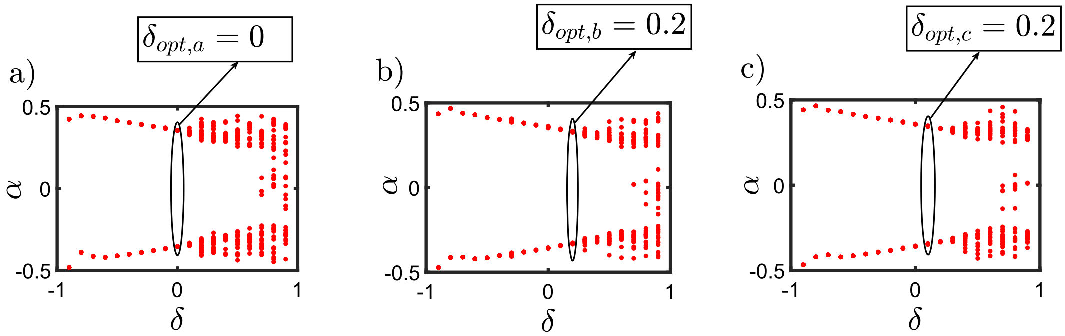

Fig. 11 Sweep results varying higher values of NES stiffness. Tuned δ values for Cases **a**, **b** and **c** in Table 5 are also identified

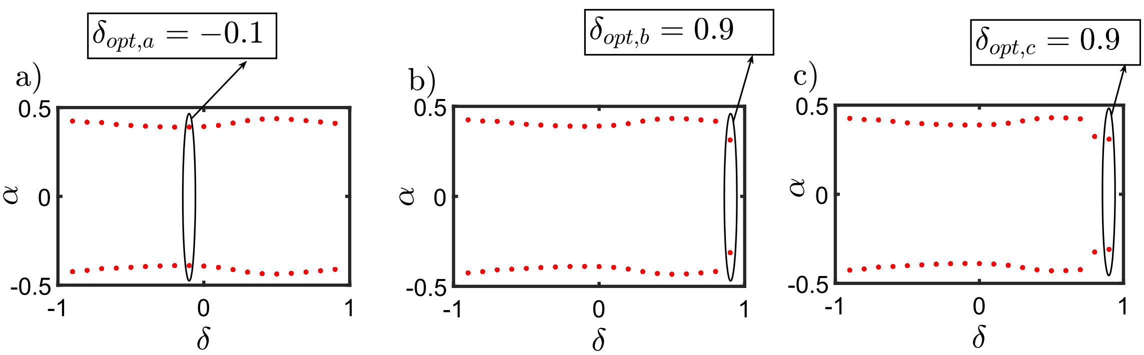

Fig. 12 Sweep Results using $\lambda_s = 0.1$ and varying high values of NES stiffness. Tuned δ values for cases **a**, **b** and **c** in Table 6 are also identified

Table 6 Parameter values for sweep with high stiffness values corresponding to Fig. 12. Minimum peak pitch amplitude is also denoted

Case	ϵ	λ_s	η_s	δ	$\min(\alpha(\tau))$ [rad]
a)	0.1	0.1	240	-0.1	0.38
b)	0.1	0.1	270	0.9	0.31
c)	0.1	0.1	290	0.9	0.30

comparative bifurcation diagram was plotted showing the coupled and uncoupled system behaviours, using flow speed as the bifurcation parameter. The results obtained are given in Fig. 13.

We observe that there is minimal suppression observed up to a flow speed of $V = 7.2$, beyond which there is a sudden decrease in LCO amplitude. A possible explanation for this could be that the activation energy threshold of the NES [52], i.e., the minimum energy level beyond which

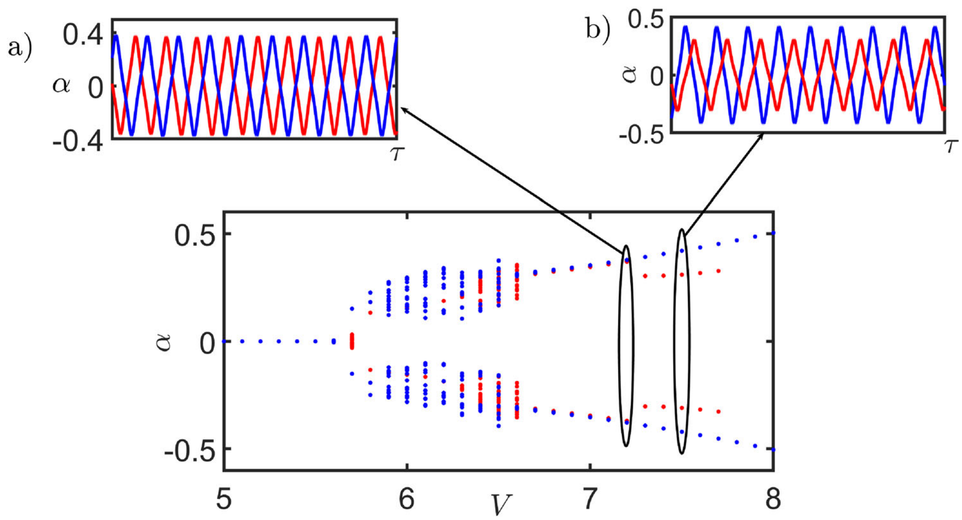

Fig. 13 Comparative bifurcation diagram after tuning NES and using values from case **c** in Table 6. Time histories of responses at **a** $V = 7.2$ **b** $V = 7.5$

Table 7 Parameter values of NES1 and NES2

ϵ_1	λ_{s1}	η_{s1}	δ_1	ϵ_2	λ_{s2}	η_{s2}	δ_2
0.1	0.1	290	0.9	0.1	0.1	290	−0.1

significant TET occurs is crossed at the flow speed of $V = 7.3$, leading to robust suppression of LCO amplitude. Energy is transferred from the primary system to the NES when their instantaneous natural frequencies match. There is, then, an energy level that is associated with that value of instantaneous frequency at which a large amount of energy is transferred.

As the NES is modeled as a spring-mass system with a cubic nonlinear stiffness, its total nondimensionalized energy can be obtained by the summation of its kinetic and potential energies [28] - i.e.,

$$E_{\mathrm{NES}} = \frac{1}{2}e(v' + \delta\alpha' - \xi')^2 + \frac{1}{4}\eta_s(v + \delta\alpha - \xi)^4 \tag{19}$$

Here, e is the nondimensional mass of the NES, and v', α' and ξ' are the NES, pitch and plunge velocities respectively. v, α and ξ are the NES, pitch and plunge displacements respectively. δ is the NES offset distance and η_s is the nondimensionalized stiffness coefficient of the NES. Using this, we plot energy time histories of the NES prior to and after crossing of the energy threshold,

The amount of energy dissipated from the NES is dependent on the amplitude of relative motion between the airfoil and NES, and it is observed that the threshold for the presented case of dynamic stall lies at V = 7.2, as we note that the total energy of the NES post $V = 7.2$ is significantly higher than prior to it, indicating that a large amount of energy is being transferred from the primary structure, i.e., the airfoil to the NES.

Next, we use the tuned NES parameters (under deterministic settings) and attempt to apply it on the airfoil subjected to randomly time-varying input wind. Suppressing or reducing the effect of random LCOs due to dynamic stall will prove extremely beneficial to the system's life as the fatigue damage incurred in stochastic cases has been shown to be significantly greater than in deterministic cases [60] and hence underscoring the need for us to undertake this exercise.

Airfoil-NES subjected to stochastic input flows

We begin the section by introducing the behaviour of the system when uncoupled with NES. The randomness in the flow is modeled using the Karhunen-Loeve expansion, and a short brief on it is provided in Sect. "The Karhunen-Loeve Expansion for Stochastic Flows". Figure 5 provides the flow profiles for a mean flow speed of $V_m = 5$. A classification of the nature of inflow considered in this work can be found in Sect. "Methodology". The results obtained are in accordance with [60].

As mentioned in Sect. "Methodology", the noise intensity is set at $\sigma = 0.3$, and the time scales are 'long', corresponding to a correlation length of 1000. Depending on the noise intensity and time scales, the response dynamics of the system can be greatly varied [60]. However, for illustrative purpose this study fixes the noise intensity and correlation length - rather than providing a range of values for the same.

In the system response when uncoupled with NES, (Fig. 15), we can observe 'on-off' type intermittency [13, 68], which consists of distinct 'on' states of high amplitude oscillations amidst 'off' states of rest/no oscillation. The amplitude of the 'on' states increases with an increase in V_m. The results of system coupled with NES are also presented for these values of V_m as here for the sake of continuity. Note that we do not study the responses of the

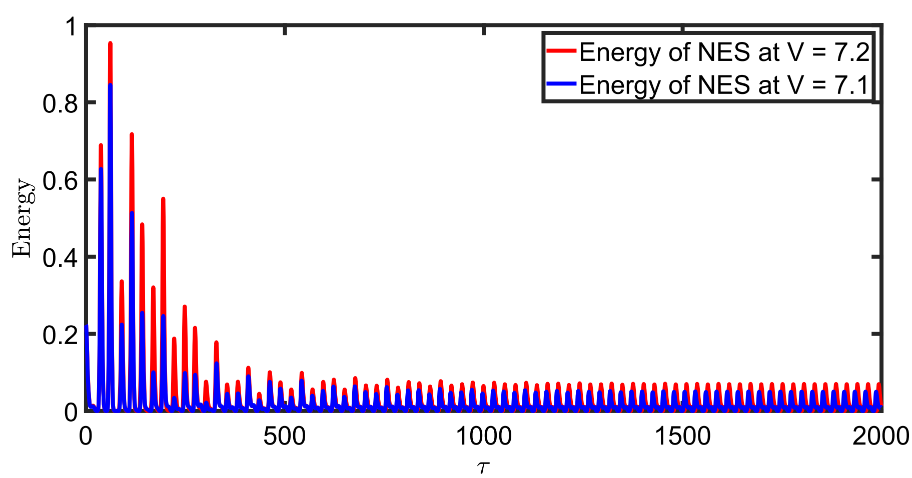

Fig. 14 Comparative energy time histories of the NES prior to and after crossing of activation energy threshold. Significant increase in energy absorbed by NES is noted

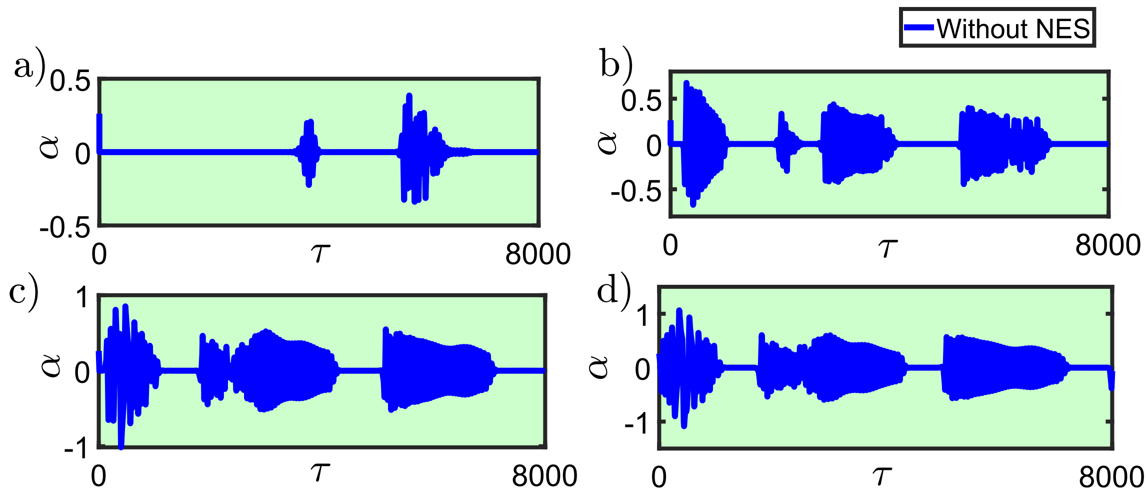

Fig. 15 Response of system without NES at (a) $V_m = 5.6$, (b) $V_m = 6$, (c) $V_m = 6.6$, (d) $V_m = 7$ for a noise intensity of $\sigma = 0.3$ and long time scale fluctuations

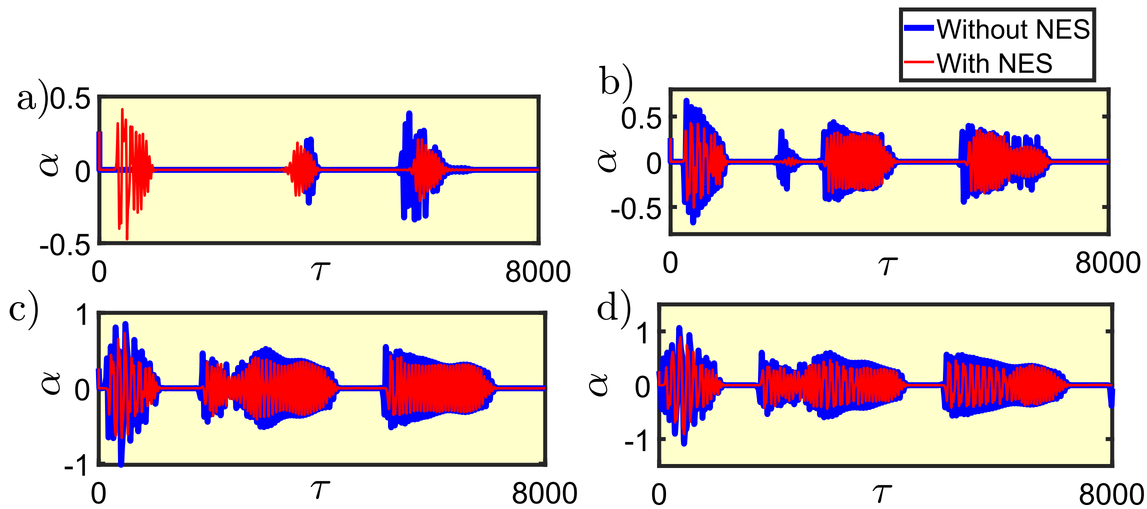

Fig. 16 Response of system coupled with NES at (a) $V_m = 5.6$, (b) $V_m = 6$, (c) $V_m = 6.6$, (d) $V_m = 7$ for a noise intensity of $\sigma = 0.3$ and long time scale fluctuations

system for higher values of V_m as the Leishman-Beddoes model is restrictive for pitch values greater than 45°.

We observe reducing amplitudes of oscillations during 'on-off' intermittent behaviour in Fig. 16. We follow the notions suggested in Venkatramani et al [13] towards the appearance of 'on-off' intermittent behaviour, i.e., the stay of $V(\tau)$ over the critical limit V_{cr} for a sufficiently long time. The cause for improved NES effectiveness may be attributed to the same, i.e., the energy extracted from the flow by the pitch mode (and consequentially its instantaneous total energy) stays in the vicinity of the threshold activation energy for a sufficiently long time allowing for the NES and airfoil to establish frequency relations and transfer energy.

The reduced amplitudes in the case of long time scale fluctuations prove that there exists merit in the use of nonlinear energy sinks in aeroelastic systems under real-life scenarios. Indeed, typical in-field wind gusts that impact wind turbine blades, helicopter blades and unmanned aerial vehicles are often long time scales [13] and extreme events such as cyclonic behavior could have rapid time variations.

It is necessary to note that the appearance of intermittent oscillatory behaviour on inclusion of the NES (in Fig. 16a) is not an artefact of the addition of the NES worsening the vibrations, but is simply an effect of the change of parameters on the dynamics of the system. The parameters influencing the appearance of intermittent oscillations in this case is dependent on the interactions of the time scales, noise intensity as well as system parameters [14]. Upon the inclusion of the NES, the overall damping of the system is subjected to change. This in turn affects the "laminar"

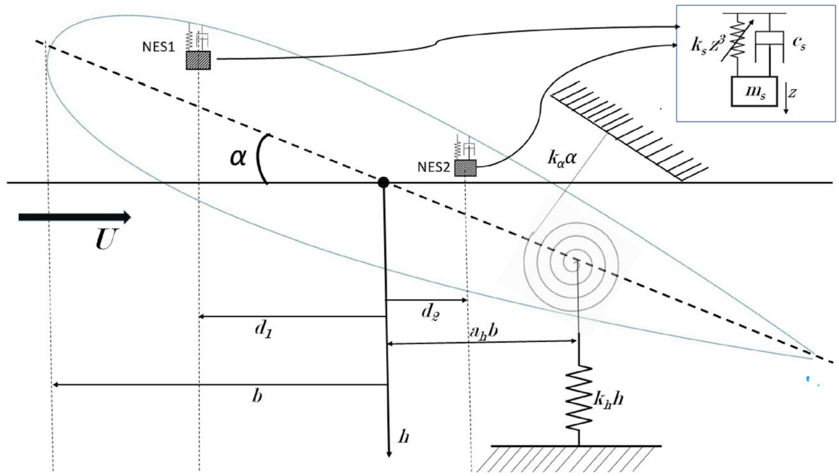

Fig. 17 A sketch of the airfoil section with two NESs attached

length of the on-off intermittent behaviour observed, that is, the occurrences of the bursts of oscillations amidst the off states [13, 69].

The implementation of NES in short time scale fluctuations is beyond the scope of this current study and is an open problem to be considered for future work owing to both the demanding computational efforts and the need to update the LB model to capture such rapid stochastic processes. The possibility of investigations into different NES configurations and their impact on suppression of random LCOs is also an interesting open problem to be studied in future work.

So far we deployed NES to an airfoil subjected to dynamic stall and showed that under both deterministic and stochastic input flows - considerable reductions in amplitudes of the oscillatory instabilities are possible. While optimizing the NES parameters seems to be the crux - we note that studying the physics of TET is still in its evolutionary stage. Given the torsionally dominant oscillatory instability stall flutter poses - we are inclined to believe that a base-line investigation to the use of multiple NESs could provide additional insights to instability suppression in aeroelastic problems. To that end, as a tail end to this paper, we present a rudimentary study involving two NESs in the next subsection. For ease of computation and understanding of the findings, the multi-NES study is presented only under deterministic flow conditions.

Preliminary Study into Multiple NESs

Zhang et. al [43] studied the targeted energy transfer between two NESs and a pitch-plunge airfoil subjected to steady-state aerodynamic loading. The motivation behind the use of two sinks was to increase the range of frequencies for which the NES suppression is effective. It was observed that in this case, the two sinks interacted with the two modes of the airfoil, i.e., one with the plunge and the other with the pitch mode. Deriving impetus from this, and duly noting that in [43] the aerodynamic model was a simplistic steady-state formulation against the complex LB formulation adopted in this work - we embark into using two NESs over the airfoil.

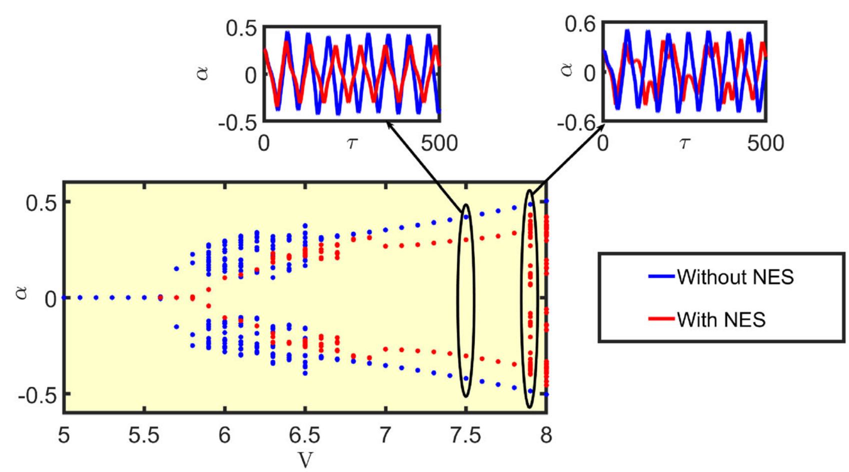

Fig. 18 Bifurcation diagram for the system with two NES oscillators

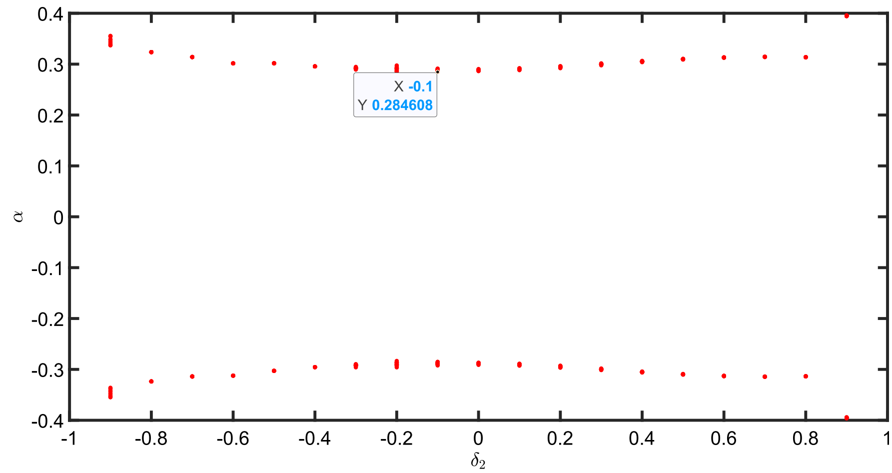

Fig. 19 Sweep of δ_2 performed to find NES2 offset. We exclude from consideration the positioning of NES1, and are able to find point of least stall flutter amplitude with two NESs

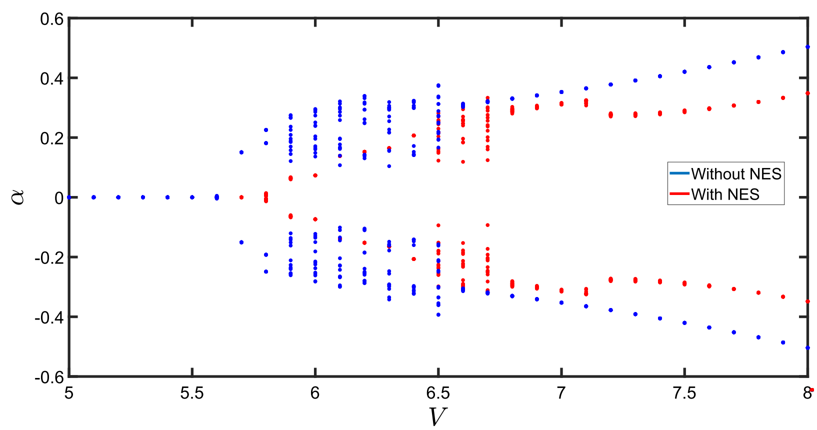

Fig. 20 Comparative bifurcation diagram of the system response with tuned δ_2, with insets of time histories of (a) Dynamics in aperiodic regime (b) Stall flutter amplitude reduction

Presented below is the mathematical model for the airfoil-multiNES system as well as the salient results observed when the system was subjected to dynamic stall.

The two NESs are placed at offset distances d_1 and d_2. Below are the equations of motion of the system.

$$\begin{cases} m\ddot{h} + S_\alpha\ddot{\alpha} + k_h h + c_{s1}(\dot{h} + d_1\dot{\alpha} - \dot{z}_1) + k_{s1}(h + d_1\alpha - z_1)^3 \\ \quad + c_{s2}(\dot{h} + d_2\dot{\alpha} - \dot{z}_2) + k_{s2}(h + d_2\alpha - z_2)^3 = -L \\ I_\alpha\ddot{\alpha} + S_\alpha\ddot{h} + k_\alpha\alpha + d_1 c_{s1}(d_1\dot{\alpha} + \dot{z}_1 - \dot{h}) + d_1 k_{s1}(d_1\alpha + z_1 - h)^3 \\ \quad + d_2 c_{s2}(d_2\dot{\alpha} + \dot{z}_2 - \dot{h}) + d_2 k_{s2}(d_2\alpha + z_2 - h)^3 = M \\ m_{s1}\ddot{z} + c_{s1}(\dot{z} + d_1\dot{\alpha} - \dot{h}) + k_{s1}(z + d_1\alpha - h)^3 = 0 \\ m_{s2}\ddot{z} + c_{s2}(\dot{z} + d_2\dot{\alpha} - \dot{h}) + k_{s2}(z + d_2\alpha - h)^3 = 0 \end{cases}$$

These equations are then nondimensionalized, and the equations are put in state-space form and ODE45 solver in MATLAB was used to solve the system of nonlinear ODEs.

$$\begin{cases} \xi'' + \chi_\alpha\alpha'' + \frac{\overline{\omega}^2}{V^2}\xi + 2\frac{\overline{\omega}}{V}\lambda_{s1}(\xi' + \delta_1\alpha' - v_1') + \frac{\overline{\omega}^2 b^2}{V^2}\eta_{s1}(\xi + \delta_1\alpha - v_1)^3 \\ \quad + 2\frac{\overline{\omega}}{V}\lambda_{s2}(\xi' + \delta_2\alpha' - v_2') + \frac{\overline{\omega}^2 b^2}{V^2}\eta_{s2}(\xi + \delta_2\alpha - v_2)^3 = -\frac{C_L}{\pi\mu} \\ \frac{\chi_\alpha}{r_\alpha^2}\xi'' + \alpha'' + \frac{1}{V^2}\alpha + 2\frac{\delta_1 b^2}{V}\lambda_{s1}(\delta_1\alpha' + v_1' - \xi') + \frac{\delta_1\overline{k}}{V^2}\eta_{s1}(\delta_1\alpha + v_1 - \xi)^3 \\ \quad + 2\frac{\delta_2 b^2}{V}\lambda_{s2}(\delta_2\alpha' + v_2' - \xi') + \frac{\delta_2\overline{k}}{V^2}\eta_{s2}(\delta_2\alpha + v_2 - \xi)^3 = \frac{2C_M}{\pi\mu r_\alpha^2} \\ \epsilon_1 v_1'' + 2\frac{\overline{\omega}}{V}\lambda_{s1}(v_1' + \delta_1\alpha' - \xi') + \frac{\overline{\omega}^2 b^2}{V^2}\eta_{s1}(v_1 + \delta_1\alpha - \xi)^3 = 0 \\ \epsilon_2 v_2'' + 2\frac{\overline{\omega}}{V}\lambda_{s2}(v_2' + \delta_2\alpha' - \xi') + \frac{\overline{\omega}^2 b^2}{V^2}\eta_{s2}(v_2 + \delta_2\alpha - \xi)^3 = 0 \end{cases}$$

The NES1 parameters were chosen using the results from the previous section, which provided us with a parameter set that displayed best suppression after tuning (see Section "Airfoil-NES Subjected to Deterministic Flows"). For NES2, the mass ratio (ϵ_2), stiffness coefficient (η_{s2}) and damping (λ_{s2}) were kept the same as NES1, and an offset of $\delta_2 = -0.5$ was chosen to obtain preliminary results. Aperiodic behaviour is observed at higher flow-speeds, as can be seen in Fig. 18. This calls for a sweep of NES offset distance to find the best location for the second NES. NES2 can be placed at any location in the airfoil except the current location of NES1, ($\delta_1 = 0.9$), and the sweep is carried out accordingly. The results of the sweep are given in Fig. 19.

From the sweep, an NES2 offset of $\delta_2 = -0.1$ is found, which is then used to get the system response. The NES1 and NES2 parameters are tabled below.

On using these parameters, the following system response was obtained. It was observed that the minimum threshold energy before strong TET occurs was slightly reduced as the NESs seemed to show better suppression at lower flowspeeds as well. Using the tuned offset distance also removed the aperiodic behaviour noted at higher flowspeeds in the preliminary case.

However, the overall reduction in amplitude with two NESs was not significantly greater than that with one NES. We also note in Fig. 20a that the delay in reaching full-fledged stall flutter results in the dynamics of the originally aperiodic regime of the baseline (without NES) case being changed to low-amplitude stall flutter oscillations. Improving and optimizing the airfoil-multiNES system could be the subject of future works, as well as testing other configurations of the NES as mentioned above in the presence of coupled structural and aerodynamic nonlinearities.

Concluding Remarks

This study focused on studying NES performance in deterministic and stochastic aeroelastic systems experiencing stall. Using systematic parametric sweeps, effective NES parameter regimes were identified and the NES was shown to be able to reduce the amplitudes of stall flutter LCOs of a pitch-plunge airfoil under deterministic conditions. From the multi-parameter sweep, we showed that there exists a regime of NES stiffness values for which efficient TET can be observed after tuning. The NES damping coefficient purely serves as a dissipator of energy localized in the NES, and a high value of the same ensures quick dissipation of localized energy. If the NES damping is not high enough, it may allow for possible leakage of energy from the NES back to the primary system, giving rise to some aperiodic behaviour as observed in the sweeps in Fig. 10a.

On obtaining the tuned NES parameters through the sweeps, a reduction of $\approx 30\%$ in peak LCO amplitude was observed.

The NES when applied in the case of stochastic loading showed a mild-success in TET, resulting in a relatively small reduction in oscillation amplitude during the 'on-off' intermittent behaviour. As a tail end to NES capabilities in suppressing stall-induced instabilities, we showed that multi-NES seem to provide almost the same extent of oscillatory amplitude suppression in comparison to its single counterpart. However, the location and parameters specific to multi-NES were not rigorously optimized, and hence this end of finding needs a cautious interpretation.

The present study is first of its kind to systematically investigate the effect of an NES in a nonlinear aerodynamic problem (dynamic stall) and present the suppression of aeroelastic (stall) flutter instability. The investigations undertaken in this paper pave the way for study into other NES configurations, many of which have been studied and can be applied to the case of dynamic stall, such as the inerter-based NES [70], and even fractional nonlinear energy sinks [71], which uses a one-third power stiffness term in the NES, which aids in reduction of the energy threshold for NES effectiveness, as well as quick energy dissipation. The applications of the same in aeroelastic problems are very interesting open problems to be considered for future works.

Acknowledgements The lead author thanks Mr. Rahul Das for insightful discussions on nonlinear energy sinks.

Funding Dr. J. Venkatramani gratefully acknowledges with gratitude the funding received from the Science and Engineering Research Board (SERB), India - core grant (CRG/2022/001609) and the institute seed grant received from Indian Institute of Information Technology Design and Manufacturing, Kancheepuram (File no IIITDM/ISG/2024/ME/02).Prof. G. Litak was supported by National Science Centre, Poland, under the project SHENG-2, No. 2021/40/Q/ST8/00362.

Data availability The numerical data used in this work can be shared upon a reasonable request to the corresponding author.

Declarations

Conflict of interest The authors declare no potential Conflict of interest with respect to the research, authorship, and/or publication of this article.

References

1. Fung YC (2008) An Introduction to the Theory of Aeroelasticity. Courier Dover Publications, New York
2. Venkatramani J, Nair V, Sujith R, Gupta S, Sarkar S (2017) Multi-fractality in aeroelastic response as a precursor to flutter. J Sound Vib 386:390–406
3. Bose C, Gupta S, Sarkar S (2019) Transition to chaos in the flow-induced vibration of a pitching-plunging airfoil at low reynolds numbers: Ruelle-takens-newhouse scenario. Int J Non-Linear Mech 109:189–203
4. Poirel D, Price SJ (2007) Bifurcation characteristics of a two-dimensional structurally non-linear airfoil in turbulent flow. Nonlinear Dyn 48:423–435
5. Abdelkefi A, Vasconcellos R, Marques FD, Hajj MR (2012) Bifurcation analysis of an aeroelastic system with concentrated nonlinearities. Nonlinear Dyn 69:57–70
6. Raaj A, Venkatramani J, Mondal S (2019) Synchronization of pitch and plunge motions during intermittency route to

aeroelastic flutter. Chaos: An Interdisciplinary Journal of Nonlinear Science **29**(4)
7. Vishal S, Raaj A, Bose C, Venkatramani J (2021) Routes to synchronization in a pitch-plunge aeroelastic system with coupled structural and aerodynamic nonlinearities. Int J Non-Linear Mech 135:103766
8. Dimitriadis G (2017) Introduction to nonlinear aeroelasticity. John Wiley & Sons, London
9. Dimitriadis G, Li J (2009) Bifurcation behavior of airfoil undergoing stall flutter oscillations in low-speed wind tunnel. AIAA J 47(11):2577–2596
10. Vishal S, Raaj A, Bose C, Venkatramani J, Dimitriadis G (2022) Numerical investigation into discontinuity-induced bifurcations in an aeroelastic system with coupled non-smooth nonlinearities. Nonlinear Dyn 108(4):3025–3051
11. Tripathi D, Shreenivas R, Bose C, Mondal S, Venkatramani J (2022) Experimental investigation on the synchronization characteristics of a pitch-plunge aeroelastic system exhibiting stall flutter. Chaos Interdiscip J Nonlinear Sci 32(7):073114
12. Pettit CL (2004) Uncertainty quantification in aeroelasticity: recent results and research challenges. J Aircr 41(5):1217–1229
13. Venkatramani J, Kumar SK, Sarkar S, Gupta S (2017) Physical mechanism of intermittency route to aeroelastic flutter. J Fluids Struct 75:9–26
14. Venkatramani J, Sarkar S, Gupta S (2018) Intermittency in pitch-plunge aeroelastic systems explained through stochastic bifurcations. Nonlinear Dyn 92:1225–1241
15. Rangarajan S, Tripathi D, Venkatramani J (2023) Non-normality and transient growth in stall flutter instability. Chaos: An Interdisciplinary Journal of Nonlinear Science **33**(3)
16. Venkatramani J, Nair V, Sujith R, Gupta S, Sarkar S (2016) Precursors to flutter instability by an intermittency route: a model free approach. J Fluids Struct 61:376–391
17. Venkatramani J, Sarkar S, Gupta S (2018) Investigations on precursor measures for aeroelastic flutter. J Sound Vib 419:318–336
18. Jonsson E, Riso C, Lupp CA, Cesnik CE, Martins JR, Epureanu BI (2019) Flutter and post-flutter constraints in aircraft design optimization. Prog Aerosp Sci 109:100537
19. Gali SV, Goehmann TG, Riso C (2023) Fundamental investigation into output-based prediction of whirl flutter bifurcations. J Fluids Struct 123:103986
20. Akshay S, Gopalakrishnan E, Sowmya V, Venkatramani J, Tripathi D, Prasad JS, Mondal S (2023) Open set domain adaptation for classification of dynamical states in nonlinear fluid dynamical systems. IEEE Access
21. Balaji PS, Karthik SelvaKumar K (2021) Applications of nonlinearity in passive vibration control: a review. J Vib Eng Technol 9:183–213
22. Baz AM (2019) Active and passive vibration damping. John Wiley & Sons, London
23. Zhang F, Soffker D (2009) Active flutter suppression of a nonlinear aeroelastic system using pi-observer. Motion and vibration control. Springer, Cham, pp 367–376
24. Kassem M, Yang Z, Gu Y, Wang W, Safwat E (2020) Active dynamic vibration absorber for flutter suppression. J Sound Vib 469:115110
25. Lee YS, Kerschen G, McFarland DM, Hill WJ, Nichkawde C, Strganac TW, Bergman LA, Vakakis AF (2007) Suppressing aeroelastic instability using broadband passive targeted energy transfers, part 2: experiments. AIAA J 45(10):2391–2400
26. Vakakis AF, Gendelman OV, Bergman LA, McFarland DM, Kerschen G, Lee YS (2008) Nonlinear targeted energy transfer in mechanical and structural systems, vol 156. Springer, Berlin
27. Verstraelen E, Habib G, Kerschen G, Dimitriadis G (2017) Experimental passive flutter suppression using a linear tuned vibration absorber. AIAA J 55(5):1707–1722
28. Das R, Bajaj AK, Gupta S (2023) Nonlinear energy sink coupled with a nonlinear oscillator. Int J Non-Linear Mech 148:104285
29. Gendelman OV (2001) Transition of energy to a nonlinear localized mode in a highly asymmetric system of two oscillators. Nonlinear Dyn 25:237–253
30. Kumar P, Narayanan S, Gupta S (2019) Targeted energy transfer in stochastically excited system with nonlinear energy sink. Eur J Appl Math 30(5):869–886
31. Jun W, Zi-Jian Y, Yun-Hao Z, Jian-Chao Z (2024) Energy transfer and dissipation in combined-stiffness nonlinear energy sink systems. J Comput Nonlinear Dyn. **19**(3)
32. Zeng Y-C, Ding H (2023) A tristable nonlinear energy sink. Int J Mech Sci 238:107839
33. Li S, Li J, Zhu H, Lai S-K (2023) Dynamical analysis and numerical verification of a non-smooth nonlinear energy sink. Int J Non-Linear Mech 151:104381
34. Ding H, Chen L-Q (2020) Designs, analysis, and applications of nonlinear energy sinks. Nonlinear Dyn 100(4):3061–3107
35. Geng X-F, Ding H, Ji J-C, Wei K-X, Jing X-J, Chen L-Q (2024) A state-of-the-art review on the dynamic design of nonlinear energy sinks. Eng Struct 313:118228
36. Lee YS, Vakakis AF, Bergman LA, McFarland DM, Kerschen G (2007) Suppression aeroelastic instability using broadband passive targeted energy transfers, part 1: Theory. AIAA J 45(3):693–711
37. Bichiou Y, Hajj MR, Nayfeh AH (2016) Effectiveness of a nonlinear energy sink in the control of an aeroelastic system. Nonlinear Dyn 86:2161–2177
38. Pidaparthi B, Missoum S (2019) Stochastic optimization of nonlinear energy sinks for the mitigation of limit cycle oscillations. AIAA J 57(5):2134–2144
39. Pérez JG, Ghadami A, Sanches L, Michon G, Epureanu BI (2022) Data-driven optimization for flutter suppression by using an aeroelastic nonlinear energy sink. J Fluids Struct 114:103715
40. Sapsis TP, Vakakis AF, Bergman LA (2011) Effect of stochasticity on targeted energy transfer from a linear medium to a strongly nonlinear attachment. Probab Eng Mech 26(2):119–133
41. Li X, Ding H, Chen L-Q (2022) Effects of weights on vibration suppression via a nonlinear energy sink under vertical stochastic excitations. Mech Syst Signal Process 173:109073
42. Wu P, Xiao J, Zhao Y (2023) Power spectrum analysis and optimization design of nonlinear energy sink under random excitation. J Vib Eng Technol. pp 1–11
43. Zhang W, Liu Y, Cao S, Chen J, Zhang Z, Zhang J (2017) Targeted energy transfer between 2-d wing and nonlinear energy sinks and their dynamic behaviors. Nonlinear Dyn 90:1841–1850
44. Kerschen G, Peeters M, Golinval J-C, Vakakis AF (2009) Nonlinear normal modes, part i: a useful framework for the structural dynamicist. Mech Syst Signal Process 23(1):170–194
45. Rana R, Soong T (1998) Parametric study and simplified design of tuned mass dampers. Eng Struct 20(3):193–204
46. Rosenberg RM (1962) The normal modes of nonlinear n-degree-of-freedom systems. J Appl Mech 29:7–14
47. Gendelman O, Manevitch LI, Vakakis AF, M'Closkey R (2001) Energy pumping in nonlinear mechanical oscillators: part i-dynamics of the underlying hamiltonian systems. J Appl Mech 68(1):34–41
48. Vakakis AF, Gendelman O (2001) Energy pumping in nonlinear mechanical oscillators: part ii-resonance capture. J Appl Mech 68(1):42–48
49. Lee YS, Vakakis AF, Bergman LA, Michael McFarland D (2006) Suppression of limit cycle oscillations in the van der pol

oscillator by means of passive non-linear energy sinks. Struct Control Health Monit 13(1):41–75
50. Vaurigaud B, Ture Savadkoohi A, Lamarque C-H (2011) Targeted energy transfer with parallel nonlinear energy sinks. part i: design theory and numerical results. Nonlinear Dyn 66:763–780
51. Ture Savadkoohi A, Vaurigaud B, Lamarque C-H, Pernot S (2012) Targeted energy transfer with parallel nonlinear energy sinks, part ii: theory and experiments. Nonlinear Dyn 67:37–46
52. Nguyen TA, Pernot S (2012) Design criteria for optimally tuned nonlinear energy sinks-part 1: transient regime. Nonlinear Dyn 69:1–19
53. Song W, Liu Z, Lu C, Li B, Fuquan N (2023) Analysis of vibration suppression performance of parallel nonlinear energy sink. J Vib Control 29(11–12):2442–2453
54. Galvanetto U, Peiro J, Chantharasenawong C (2008) An assessment of some effects of the nonsmoothness of the leishman-beddoes dynamic stall model on the nonlinear dynamics of a typical aerofoil section. J Fluids Struct 24(1):151–163
55. Guo H-l, Chen Y-S, Yang T-Z (2013) Limit cycle oscillation suppression of 2-dof airfoil using nonlinear energy sink. Appl Math Mech 34(10):1277–1290
56. Larsen JW, Nielsen SR, Krenk S (2007) Dynamic stall model for wind turbine airfoils. J Fluids Struct 23(7):959–982
57. Leishman J (1988) Validation of approximate indicial aerodynamic functions for two-dimensional subsonic flow. J Aircr 25(10):914–922
58. LEISHMAN J (1989) State-space model for unsteady airfoil behavior and dynamic stall. In: 30th Structures, Structural Dynamics and Materials Conference, p. 1319
59. Devathi H, Sarkar S (2016) Study of a stall induced dynamical system under gust using the probability density evolution technique. Comput Struct 162:38–47
60. Tripathi D, Vishal S, Bose C, Venkatramani J (2022) Stall-induced fatigue damage in nonlinear aeroelastic systems under stochastic inflow: numerical and experimental analyses. Int J Non-Linear Mech 142:104003
61. Malatkar P, Nayfeh AH (2007) Steady-state dynamics of a linear structure weakly coupled to an essentially nonlinear oscillator. Nonlinear Dyn 47:167–179
62. Jiang X, McFarland DM, Bergman LA, Vakakis AF (2003) Steady state passive nonlinear energy pumping in coupled oscillators: theoretical and experimental results. Nonlinear Dyn 33:87–102
63. Vakakis AF, Bergman LA (2008) Rebuttal of steady state dynamics of a linear structure weakly coupled to an essentially nonlinear oscillator. Nonlinear Dyn 53(1–2):167–168
64. Malatkar P, Nayfeh AH (2008) Steady state dynamics of a linear structure weakly coupled to an essentially nonlinear oscillator. Nonlinear Dyn. 47(2007):167–179
65. Tripathi D, Mondal S, Venkatramani J (2023) Frequency-specific phase synchronization analysis of a stall-induced aeroelastic system undergoing 2: 1 internal resonance in a low-speed wind tunnel. Nonlinear Dyn 111(14):12899–12920
66. Guo H, Cao S, Yang T, Chen Y (2018) Aeroelastic suppression of an airfoil with control surface using nonlinear energy sink. Nonlinear Dyn 94:857–872
67. Fasihi A, Shahgholi M, Ghahremani S (2022) The effects of nonlinear energy sink and piezoelectric energy harvester on aeroelastic instability of an airfoil. J Vib Control 28(11–12):1418–1432
68. Bethi RV, Gali SV, Venkatramani J (2020) Response analysis of a pitch-plunge airfoil with structural and aerodynamic nonlinearities subjected to randomly fluctuating flows. J Fluids Struct 92:102820
69. Kumar SK, Sarkar S, Gupta S (2019) Multiplicative noise induced intermittency in maps. Int J Non-Linear Mech 117:103251
70. Zhang Z, Lu Z-Q, Ding H, Chen L-Q (2019) An inertial nonlinear energy sink. J Sound Vib 450:199–213
71. Zhang S, Zhou J, Ding H, Wang K, Xu D (2023) Fractional nonlinear energy sinks. Appl Math Mech. 44(5):711–726